

# Modeling the effects of Southeast Asian monsoon outflow on subtropical anticyclones and midlatitude ozone over the Southern Indian Ocean

Marek Rogal,<sup>1</sup> Matthew H. Hitchman,<sup>1</sup> Marcus L. Buker,<sup>2</sup> Gregory J. Tripoli,<sup>1</sup> Ivanka Stajner,<sup>3</sup> and Hiroo Hayashi<sup>4</sup>

Received 10 August 2009; revised 13 June 2010; accepted 21 June 2010; published 19 October 2010.

[1] This observational and modeling study explores how the Southeast Asian summer monsoon outflow into the Southern Indian Ocean influences the life cycle of local anticyclones and leads to changes in the distribution of column ozone in the Southern Hemisphere (SH). A case study of the evolution of synoptic fields during August 1998 was performed to characterize the circulation leading to the average column ozone distribution known as the “ozone croissant,” with a characteristic ozone maximum south of Australia and a minimum near South America. During this month, five phases of SH circulation were found to lead to distinctive ozone patterns, explaining the monthly location and extent of the SH column ozone maximum. An isentropic trajectory model was used to show the cross-equatorial flow from the Tibetan High into the SH at the near-tropopause level of 360 K. Outflow pulses are shown to be responsible for the amplification of observed anticyclones over the SH Indian Ocean and intensification of troughs south of Australia. This couplet establishes an ozone transport pathway from tropical lower stratospheric regions around the edges of anticyclones into the ozone maximum in the amplified troughs. An idealized modeling experiment using the University of Wisconsin–Madison Nonhydrostatic Modeling System was performed to model strong outflow pulse from tropical convection. Together with model trajectory computations, the modeling study showed a strong anticyclonic response over the Indian Ocean and increased ozone transport into the amplified troughs in a perturbed wave pattern.

**Citation:** Rogal, M., M. H. Hitchman, M. L. Buker, G. J. Tripoli, I. Stajner, and H. Hayashi (2010), Modeling the effects of Southeast Asian monsoon outflow on subtropical anticyclones and midlatitude ozone over the Southern Indian Ocean, *J. Geophys. Res.*, 115, D20101, doi:10.1029/2009JD012979.

## 1. Introduction

[2] It has been observed that transient wave activity in the upper troposphere/lower stratosphere (UTLS) strongly modulates total column ozone through horizontal and vertical advection [Andrews *et al.*, 1987; Trenberth, 1992; Orsolini *et al.*, 1995, 1998; Randel and Cobb, 1994; Randel and Park, 2006]. There is a high correlation between total ozone and tropopause pressure in middle latitudes on synoptic time scales [Schubert and Munteanu, 1988; Hudson *et al.*, 2003; Wirth, 1991, 1993]. Long-term observations of column ozone in the SH show an anthropogenic ozone minimum or “ozone hole” [London *et al.*, 1976; Solomon *et al.*, 1986;

Newman and Randel, 1988; Randel *et al.*, 2002] situated over Antarctica and surrounded by an asymmetric total ozone maximum in latitudes 40–60°S. This maximum, recurrent during the southern winter and spring, is centered south of Australia and spans a longitudinal band of about 200° (Figure 1a). The core of ozone maximum (365 DU or more) is climatologically collocated with the deep trough residing over the southeastern Indian Ocean (Figure 1b) during most part of late winter and spring in the SH. The western stretch of 335 DU isoline trails closely the climatological trough observed at the 150 hPa level (between 0° and 120°E) while also stretching into area dominated by pronounced ridge southeast of Australia (between 120°E and 120°W). Seasonal and ENSO variability are explored in separate manuscripts [Hitchman and Rogal, 2010a, 2010b]. Hitchman and Rogal [2010a] focuses on seasonal changes in convection over Southeast Asia and the Maritime Continent, as well as the eastward shift in the ozone maximum that occurs during the August–October period.

[3] Classical theory of SH wave-mean flow dynamics does not fully explain the mechanisms governing such a pronounced zonal asymmetry in the ozone distribution, with

<sup>1</sup>Atmospheric and Oceanic Sciences Department, University of Wisconsin–Madison, Madison, Wisconsin, USA.

<sup>2</sup>Department of Geography, Western Illinois University, Macomb, Illinois, USA.

<sup>3</sup>Noblis, Falls Church, Virginia, USA.

<sup>4</sup>Research Institute for Sustainable Humanosphere, Kyoto University, Kyoto, Japan.

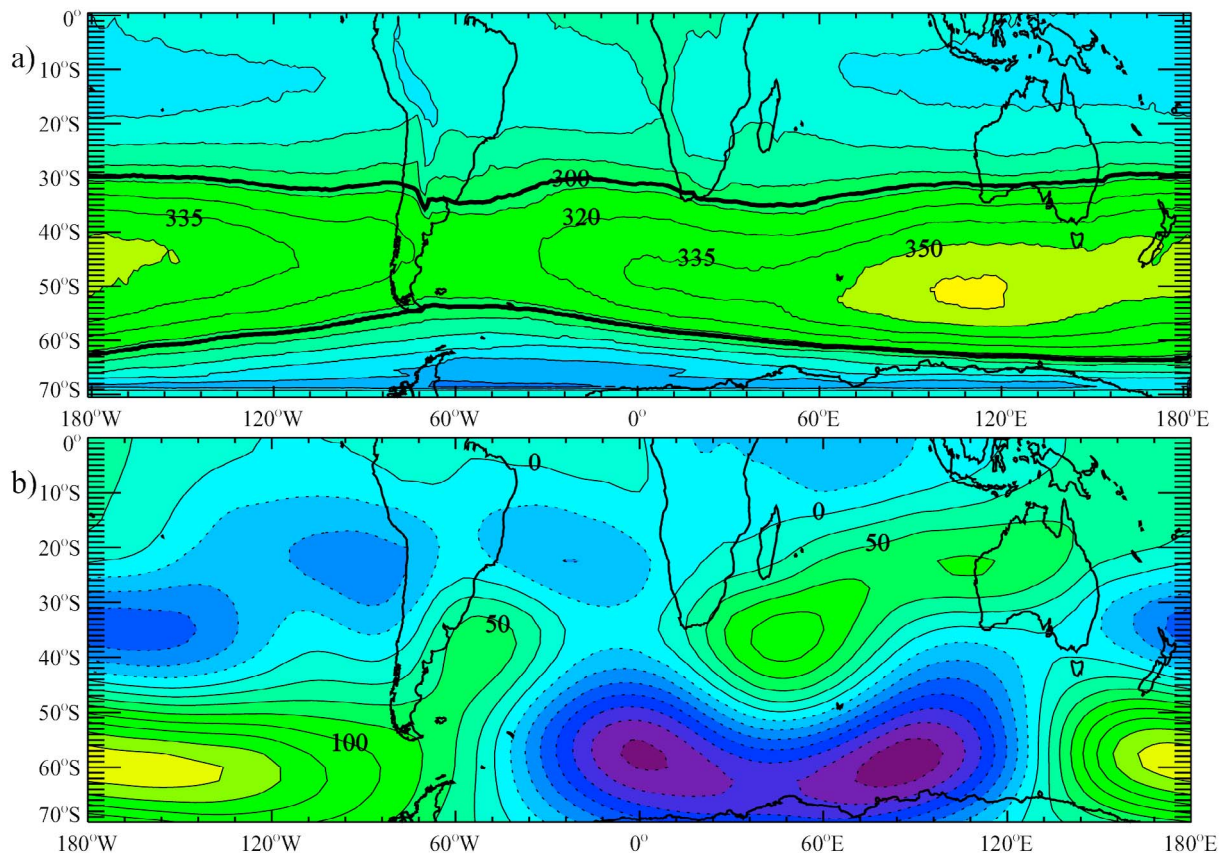


**Figure 1.** Monthly mean (a) TOMS column ozone in August 1995–2004 and (b) geopotential height anomalies at 150 hPa in August 1995–2004. Contour interval in Figure 1a is 15 Dobson Units (DU) and 25 m in Figure 1b. The 300 DU contour is thickened for easier recognition. Green and blue shades in Figure 1a represent lower values of total ozone.

such a specific seasonal and longitudinal signal. Previous studies by *Wirth* [1991, 1993] showed high correlation with the climatological structure of lower stratospheric temperature, which exhibits similar behavior to column ozone. The distribution of ozone is determined through a combination of dynamical and photochemical processes. This manuscript focuses on a synoptic case study during August 1998 that describes the dynamical precursors and events leading to the prevalent positioning of the ozone maximum (OM) south of Australia and analyzes the influence of coupling between the Tibetan High (TH) and Australian High (AH) on dynamical ozone redistribution in the SH.

[4] The main part of the hypothesis under consideration is that this ozone maximum is partially attributable to the dynamical coupling between the Northern Hemisphere's (NH) Tibetan High and the SH synoptic wave regime (TH-AH coupling). Outflow from the Tibetan High in the UTLS extends southwestward across the Indian Ocean during most of the boreal summer and fall. This phenomenon occurs at the top of the summer monsoon in Southeast Asia during the mature state and is linked to oscillations in circulation and deep convection with timescales of roughly 10–20 days during the active/break cycles [*Krishnamurti and Bhalme, 1976; Krishnamurti and Ardanuy, 1980; Randel and Park, 2006*]. Manifestations of the TH outflow may be seen in Figure 2, as predominantly southward pulses

of the meridional wind component at the position of the Singapore/Changi WMO weather station (1°22' N, 103°59' E), as seen in winds interpolated from analyses from the European Centre for Medium-Range Weather Forecasts (ECMWF). The asterisks in Figure 2 denote the times of strongest amplification of the TH, while arrows point to the time lag of 2–3 days between the buildup of the TH and the intensification of its outflow into the SH.

[5] The hypothesis is that, upon arrival in the SH, air masses from the outflow, which have anomalously positive potential vorticity (PV), spin up anticyclonically, interfere with the anticyclonic features projecting onto the local wave pattern and disturb the planetary wave pattern. A preferential longitudinal band of higher-column ozone values is created once the anticyclones over the Indian Ocean and Australia are spun-up by the TH outflow, producing a magnified trough south or southwest of the Australian Subtropical Westerly Jet, which helps to amplify the downward tropopause excursions downstream and leads to enhanced transport of the ozone-rich air parcels into it. This outflow from the circulatory system of the Tibetan High is driven in pulses on quasi-weekly time scales. Outflow pulses from the Southeast Asian monsoon occur at different longitude bands from Africa to Australia.

[6] An explanation of the TH and AH was first proposed by *Gill* [1980], with precursory work by *Webster* [1972] and

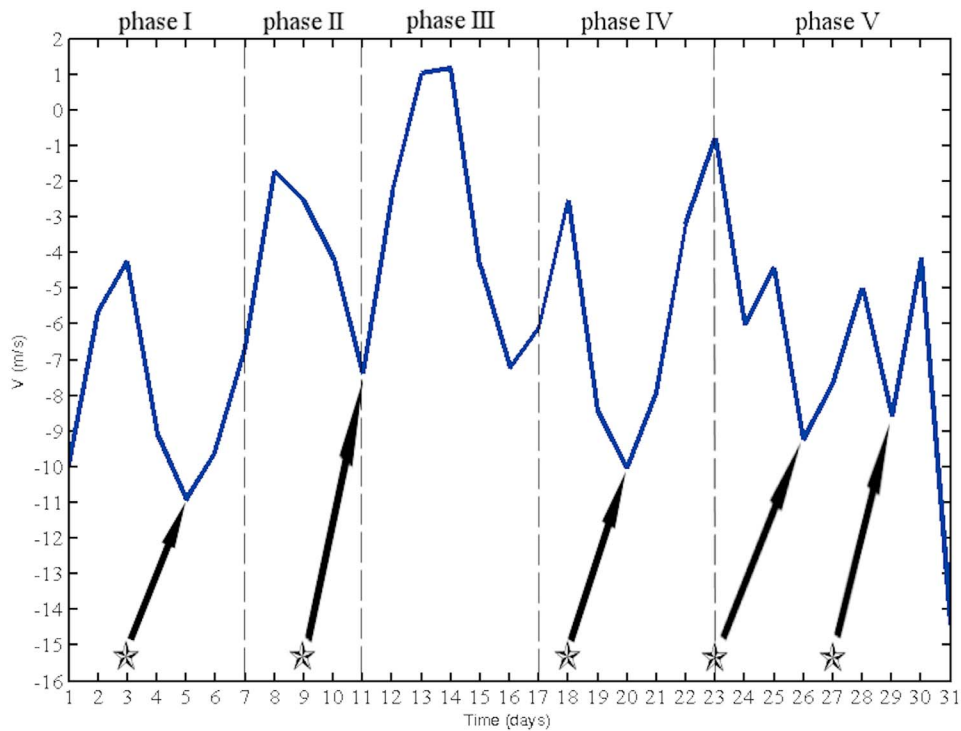


**Figure 2.** Meridional wind component (m/s) at Singapore ( $1^{\circ}22'N$ ,  $103^{\circ}59'E$ ) extracted from daily European Centre for Medium-Range Weather Forecasts (ECMWF) data at 1200 UT for August 1998 at 150 hPa.

was explored further by *Hoskins and Rodwell* [1995]. Their coupling, constituting the main factor attributing to the prevalent ozone maximum position over the southern Indian Ocean, is consistent with the dynamical structure forced by transient off-equatorial heating associated with monsoon convection. Conditions similar to those shown in Figures 1 and 2 occur during August–October in all years examined by authors in a separate manuscript describing a climatology of TH–AH coupling and total ozone redistribution in the SH during the years 1995–2004. Note the permanent existence of the AH in Figure 1b. This net of dynamical connections, starting with the TH–AH coupling, is thoroughly analyzed in a composite case study in section 3. This is further reinforced by the large-scale ozone convergence calculations for each of the composite case’s temporal subsets in section 4.

[7] In order to investigate the specific conditions leading to the climatological structure of the distribution of ozone, we have analyzed the synoptic situation observed during August 1998 and compared 3D ozone convergence patterns at 150 hPa with the evolution of synoptic-scale column ozone anomalies. One of the major advantages of calculated ozone convergence patterns is the ability to identify geographical locations with prevalent convergence of high ozone content air and to localize perpetual lower-ozone content zones at 150 hPa.

[8] The case study is reinforced by trajectories showing the origins of air parcels entering the Australian Subtropical Westerly Jet (ASWJ) on 5 August 1998. In order to qualitatively characterize the TH–AH coupling, we have employed the NASA Langley Research Center (LaRC) 3-D trajectory

model. A back-trajectory study performed with this model showed the origins of several “patches” of air masses being well within the NH at the shedding edges of an active TH. These air masses are shown to be responsible for the amplification of the AH. Separate trajectories using full model physics show the origins of the ozone rich air leading to the pronounced column ozone maximum.

[9] The observational and back-trajectory modeling analysis is followed by a modeling study, in which we have recreated the theoretical TH–AH coupling through use of the University of Wisconsin–Madison Nonhydrostatic Modeling System (UWNMS), initialized with ozone from the NASA Goddard Global Modeling and Assimilation Office (GMAO). A control run for the inflow surge in early August 1998 captured the essence of the dynamical regime associated with ozone transport, which, over time, leads to the climatological ozone crossant. A back-trajectory study was performed with UWNMS model physics to pinpoint spatial origins of the ozone arriving in the trough southeast of the AH from far upstream in the subtropical stratosphere. Section 6 contains a comparison between the control run and a perturbed run (with the inflow surge amplified) to highlight the dynamical mechanism, and includes a full discussion of the results.

## 2. Model, Data, and Methods

[10] The analysis presented in this paper was performed using  $2.5^{\circ}$  gridded global surface and upper air analyses from ECMWF [*Trenberth*, 1992; *Hollingsworth et al.*, 1986] for meteorological fields. August 1998 was split into five

phases: 1–7, 8–11, 12–17, 18–23, and 24–31 August by inspection of the location and strength of anticyclones over the South Indian Ocean (SIO) in Figure 5a. Subsets were created to enable us to evaluate the synoptic situation characterizing different regimes. These regimes consist of the presence of the AH alone, the South African High (SAH) alone, and the AH together with the IOH.

[11] The column ozone data set used in conjunction with ECMWF data is a product of the Total Ozone Mapping Spectrometer (TOMS) series. The particulars of this widely used data set may be found at <http://toms.gsfc.nasa.gov>. We have used 3-D ozone assimilation data from the NASA GMAO in order to initialize the UWNMS model with ozone acting as a tracer and to construct an ozone budget [Stajner and Wargan, 2004; Stajner et al., 2001, 2006].

[12] The ozone budget at a given altitude is given by the chemical constituent transport equation:

$$\frac{\partial n}{\partial t} + \vec{\nabla} \cdot (\vec{v}n) = (P - L) \quad (1)$$

where  $n$  is ozone mixing ratio in parts per million by volume (ppmv) and the right side (production-loss) represents photochemical sources and sinks. Daily ozone fluxes were calculated using fourth-order differencing at standard pressure levels in the layer 500–50 hPa for August 1998. The right side (production-loss) is negligible since the photochemical lifetimes for ozone in the winter UTLS were found to be on the order of weeks to months [Brasseur and Solomon, 1989] thus the photochemical terms and time rate of change were not computed; the convergence patterns are emphasized here. The sum of horizontal and vertical flux convergences at 150 hPa is compared with the ozone distribution for each subperiod defined above.

[13] The LaRC trajectory model [Pierce and Fairlie, 1993] was used to perform back-trajectory experiments. Three dimensional trajectory paths were computed using the fourth-order Runge-Kutta time step scheme [Butcher, 1987], with the time step kept at 20 min to ensure computational stability. Horizontal winds were linearly interpolated in time and space to trajectory positions.

[14] The core of the modeling study presented in section 4 is the UWNMS. The original purpose of this model [Trioli, 1992; Pokrandt et al., 1996] was to study mesoscale and synoptic-scale tropospheric phenomena such as tropical cloud clusters, lake effect snow storms, gravity waves, cyclogenesis and mesoscale convective complexes. Its variable vertical resolution makes it useful to study a variety of problems in the UTLS [Huesmann and Hitchman, 2001; Postel and Hitchman, 2001; Harvey et al., 2004], and its limited domain allows for the use of forcing by inflow from the side.

[15] The model was employed in a “hemispheric” mode, with its domain stretching over most of the SH. We initialized the model using ECMWF data interpolated to the  $85 \times 85 \times 30$  grid ( $\sim 200$  km horizontal and  $\sim 1$  km vertical resolution), with the domain centered over the South Pole. To study the ozone transport problem, we initialized the model with 3-D ozone assimilation data from the GMAO, described before in association with the ozone budget. GMAO ozone was interpolated to the ECMWF grid and then used to initialize the UWNMS and update ozone values along its boundaries.

[16] The time step of integration was 90 s. The domain sidewalls were updated every hour with temporally interpolated ECMWF and GMAO data, while flow structures were allowed to evolve in the interior of the model. Although GMAO ozone provides realistic distributions of this constituent, it was treated as a passive tracer in the UWNMS. The problem of possible reflections from the upper rigid-lid boundary at 30 km was eliminated with a Rayleigh friction “sponge layer” in the five uppermost levels. The simulation dates chosen span 1–8 August 1998, corresponding to an amplification and decay cycle of the coupled TH-AH duet.

[17] To model the cross-equatorial influence of the TH on the SH dynamical structure, several experiments with different parameterizations were performed. Perturbation of the wind field was assessed as the most promising and direct parameterization for modeling outflow from the TH. The wind field was relaxed to a northeasterly wind,  $\vec{v}' = (-10 \text{ m/s}, -20 \text{ m/s})$  in the area of maximum perturbation at  $5^\circ\text{S}, 90^\circ\text{E}$  over the SIO (see the lower right corner of Figure 9a) by adding term (2) to the model’s horizontal equations of motion:

$$-\frac{[\vec{v} - \vec{v}' \cdot S]}{\tau} \quad (2)$$

where  $\tau$  is a relaxation time scale of 0.5 days and  $S$  describes the shape of the perturbation:

$$S(x, y, z) = \exp \left[ -\left(\frac{(x - 85)}{20}\right)^2 - \left(\frac{(y - 1)}{10}\right)^2 - \left(\frac{(z - 15)}{3}\right)^2 \right] \quad (3)$$

The point  $(x, y) = (1, 1)$  is at the lower left corner. Note the Gaussian half-widths of 20 grid points in the  $x$  direction, 10 in the  $y$  direction and 3 in the vertical. The maximum perturbation is centered at 15 km, diminishing to less than 2% of the maximum amount at 9 km and 21 km. The spatial profile of the perturbation allowed for the reconstruction of very broad cross-equatorial inflow, with a width of around 4000 km in the middle of the SIO.

[18] The UWNMS was run unforced for 24 h to provide stable dynamical conditions. Subsequently, the wind perturbation was spun up in a Gaussian fashion to its maximum value at the end of day two and was kept constant between days 3–5, then linearly diminished to zero between the end of days 5 and 7. The 6 day period of wind perturbation influence was chosen to resemble the observed characteristic duration of a strong direct outflow pulse from a UTLS monsoon. By directly injecting air into the SH, we simulated an event of strong and longitudinally limited flow in the SIO. A control run was performed with no inflow parameterization, and compared to the perturbed run in order to highlight the effects of inflow.

### 3. Time Evolution and Case Analysis of Geopotential Height and Ozone Anomalies and During August 1998

[19] Dynamical interactions among the TH, AH, other SH anticyclones and the distribution of ozone are analyzed in

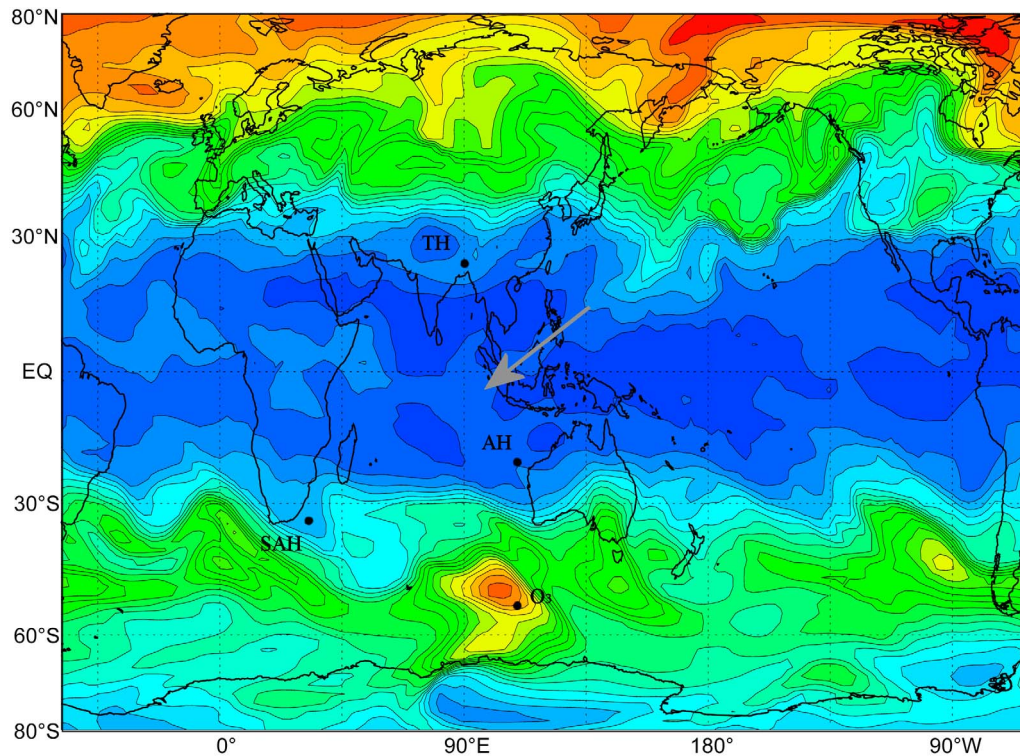


**Figure 3.** NASA Goddard Global Modeling and Assimilation Office ozone mixing ratio at 100 hPa on 4 August 1998, contour interval 0.08 ppmv, with values ranging from 0.055 to 1.8 ppmv. The maximum value in the trough southwest of Australia is 1.63 ppmv.

the following composite case study and further reinforced by large-scale ozone convergence calculations for each of the composite case's temporal subsets.

[20] An example of the effects of one such outflow event, associated with TH-AH coupling, on the distribution of ozone mixing ratio at 100 hPa from 4 August 1998, is shown in Figure 3. There is a pronounced ozone mixing ratio maximum in a trough southwest of Australia. This is immediately adjacent to the low-ozone anticyclones south of Madagascar and over northwestern Australia. Outflow surges occur in association with a stronger AH, a quasi-stationary system which resides climatologically over northwestern Australia during late winter and early spring. It may be seen in Figure 4a as a quasi-constant patch of high positive Montgomery stream function anomaly near 13°S and 80–160°E.

[21] Figure 4b shows that the AH and TH near 23°N, 100–140°E tend to amplify at similar times, coinciding with strengthened southwestward flow toward the southern Indian Ocean. Both highs are amplified on 3, 9, 18 and 23 August, notably when amplification occurs in the eastern part of the TH (coamplification dates are marked by stars on the Figure 4b). The correlation coefficient between geopotential height at 13°S, 108°E (Figure 4a) and 20°N, 90°E (Figure 4b) calculated for period of 10 years (1995–2004) at lags ranging from 0 to 9 days is in the range of 0.4–0.7 (Table 1). The highest correlation coefficient reaches 0.83 at the time lag of 2 days and is  $\sim 0.5$  for other time lags. This indicates that 2 days is a typical time lag for the transfer of anomalous vorticity air masses from the TH system into the SH. Similarly, high correlation coefficients result from

calculation using the two points associated with the AH and TH and column ozone at 50°S, 108°E (C). The time lag of 5–6 days needed to achieve good correlation between points B (TH) and C (OM) accounts for the time needed for amplification of the AH by the TH outflow (2 days) and further barotropic Rossby-wave energy dispersion downstream. The amplification of the trough immediately south of Australia allows for enhanced transport of the ozone richer air masses from the tropical and subtropical regions upstream into it within 1–2 days of magnification. The correlation coefficients calculated from geopotential height time series in the AH (Figure 4a) and column ozone in OM (Figure 4c) show a strong response of the OM to amplification of the AH, with highest values occurring at time lags of 1 to 3 days, decreasing for higher time lags and reaching low negative correlation for the time lag of 9 days.

[22] The division of August 1998 into 5 distinctive phases enables us to distinguish between the different synoptic regimes in the SH, which are visible in Figure 6 (Figures 5b–5d are described below). The monthly mean Mercator projection of ECMWF geopotential height anomalies at 150 hPa (Figure 6a) makes it possible to define the AH, centered at 25°S, 120°E, as well as the SAH-South Indian Ocean High (SIOH) system, stretching across most of the southern Indian Ocean. The northeast-southwest tilting trough over the higher-latitude SIO and the ridge southeast of Australia play important roles in our analysis, although their area is amplified significantly by the projection. This structure is compatible with radiation of Rossby wave energy from the subtropics [Sardeshmukh and Hoskins, 1988]. The month of August 1998 was divided into five

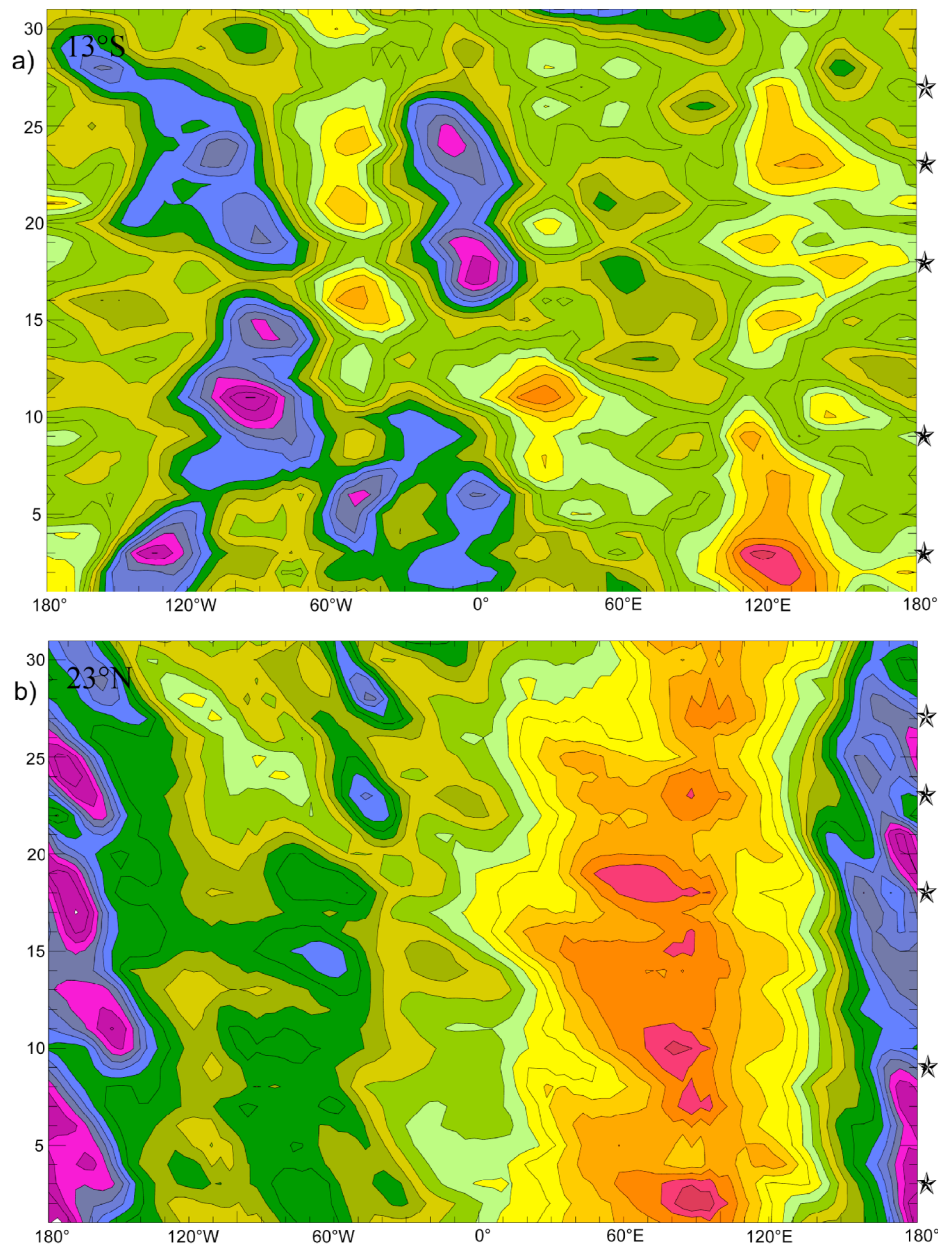


**Figure 4.** Hovmöller (longitude-time) plot of ECMWF Montgomery stream function at 360 K at (a) 13°S and (b) 23°N during August 1998. The contour interval is 100 m<sup>2</sup>/s in Figure 4a and 200 m<sup>2</sup>/s in Figure 4b. The stars indicate contemporaneous amplification of the Tibetan High and Australian High.

distinguishable phases according to Figure 5a, depending on the position and relative strength of subtropical anticyclones at 150 hPa, 20°S, including the AH, IOH and SAH (Figure 6a). Positive height differences of at least 50 m were used as a threshold identifying dominant anticyclones. Phases I and V were marked by the relatively magnified AH system, with lesser presences of the IOH and SAH (Figures 6b and 6f). Phase II has shown a weakening of both the AH and IOH (Figure 6c), while a relatively strong SAH system was observed during the phase III (Figure 6d). The main feature of phase IV (Figure 6e) was the enhanced IOH system dominating the southern extratropics in the eastern SH.

[23] These phases are distinguishable also in terms of southerly flow into the SH near Singapore (Figure 2) as well as in Hovmöller diagrams of Montgomery stream function anomalies at 13°S (Figure 4a) and in the vicinity of the TH at 23°N (Figure 4b). There is a 2–3 day lag between the magnification of the TH and the amplification of the southward flow (see stars in Figure 2 indicating amplification times of the TH, as in Figure 4b, with arrows pointing to the maximum flow magnitude). Each phase contains period of TH buildup and resulting outflow magnification, notably stronger during the phases I and IV. Phase V undergoes two such cycles within shorter periods resulting from weaker but more frequent TH intensification during

**Table 1.** Time-Lagged Correlation Coefficients Between Geopotential Heights<sup>a</sup>

Time Lag (Days)	TH-AH	AH-SAH	AH-OM	TH-OM
0	0.04	0.36	0.47	0.44
1	0.50	0.52	<b>0.66</b>	0.42
2	<b>0.83</b>	0.63	<b>0.72</b>	0.42
3	0.43	0.62	0.55	0.40
4	0.50	0.55	0.37	0.45
5	0.54	0.54	0.30	<b>0.55</b>
6	0.52	0.51	0.13	<b>0.57</b>
7	0.49	0.29	0.01	0.49
8	0.47	0.08	-0.10	0.49
9	0.49	0.06	-0.12	0.48

<sup>a</sup>At points denoted as TH (23°N, 90°E), AH (20°S, 108°E), SAH (35°S, 35°E), and the column ozone at the location 53°S, 108°E denoted as the OM. Time series include data values in July–October during the 1995–2004 period. Boldface denotes maximum values mentioned in section 3.

that period. This temporal lag of 2 days between the development of the TH (Figure 4b) and strengthening of the southward flow (Figure 2) modulating the AH (Figure 4a) was seen in statistical correlations (Table 1). High latitudes in phases I and V display stronger response to the tropical perturbation by the TH outflow and an enhanced ozone buildup in the magnified trough southwest of Australia.

[24] In phase I, 1–7 August, only one anticyclonic center (the AH) exists over the Indian Ocean and Australia region (60–140°E) (see Figures 5a and 6b). Because of the dominant position of the AH system during this phase and its significance to the climatological asymmetry in the column ozone through the transport of ozone-rich air masses into the trough immediately to the south and southeast of the AH, we chose this phase for more thorough exploration in mesoscale modeling study that is described in section 5.

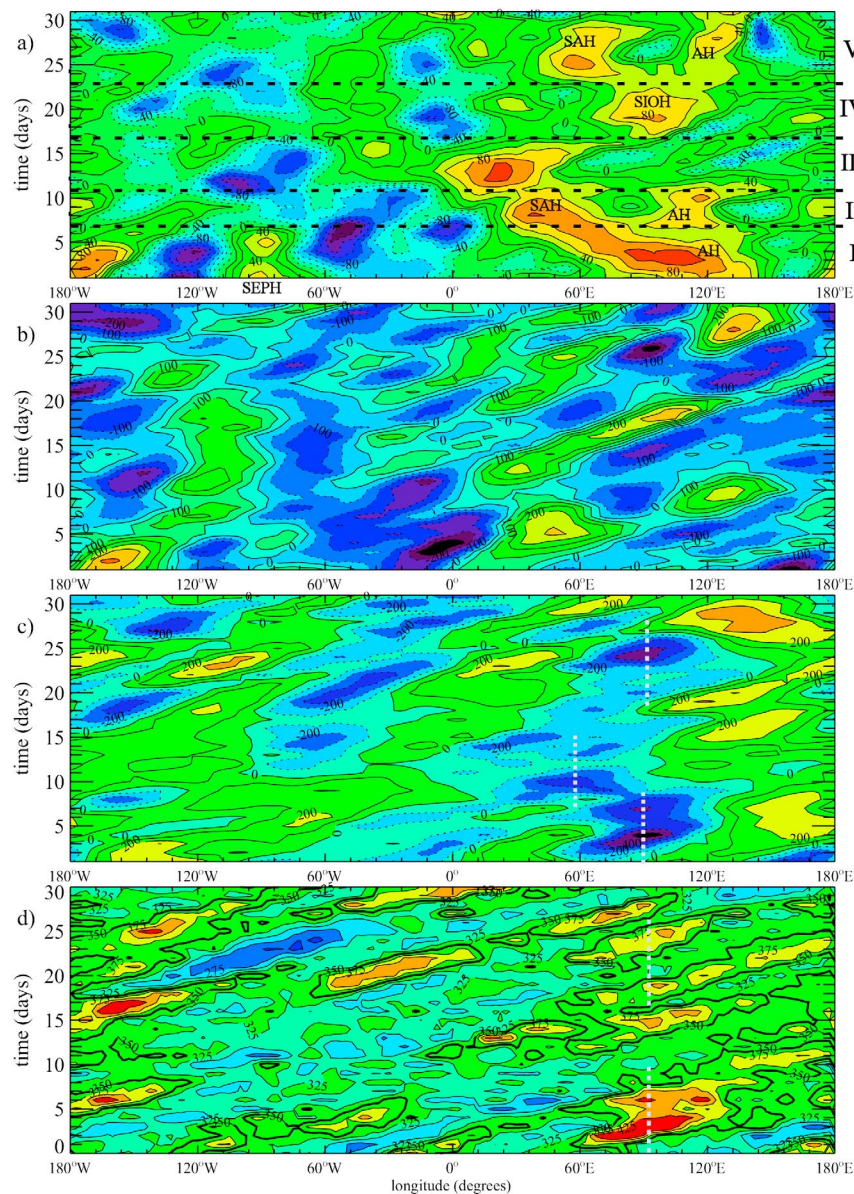


**Figure 5.** Hovmöller (longitude-time) plot of ECMWF geopotential height anomalies at 150 hPa at (a) 20°S, (b) 35°S, (c) 50°S, and (d) column ozone at 60°S during August 1998. The contour interval is 20 m in Figure 5a, 50 m in Figure 5b, 100 m in Figure 5c, and 25 DU in Figure 5d.

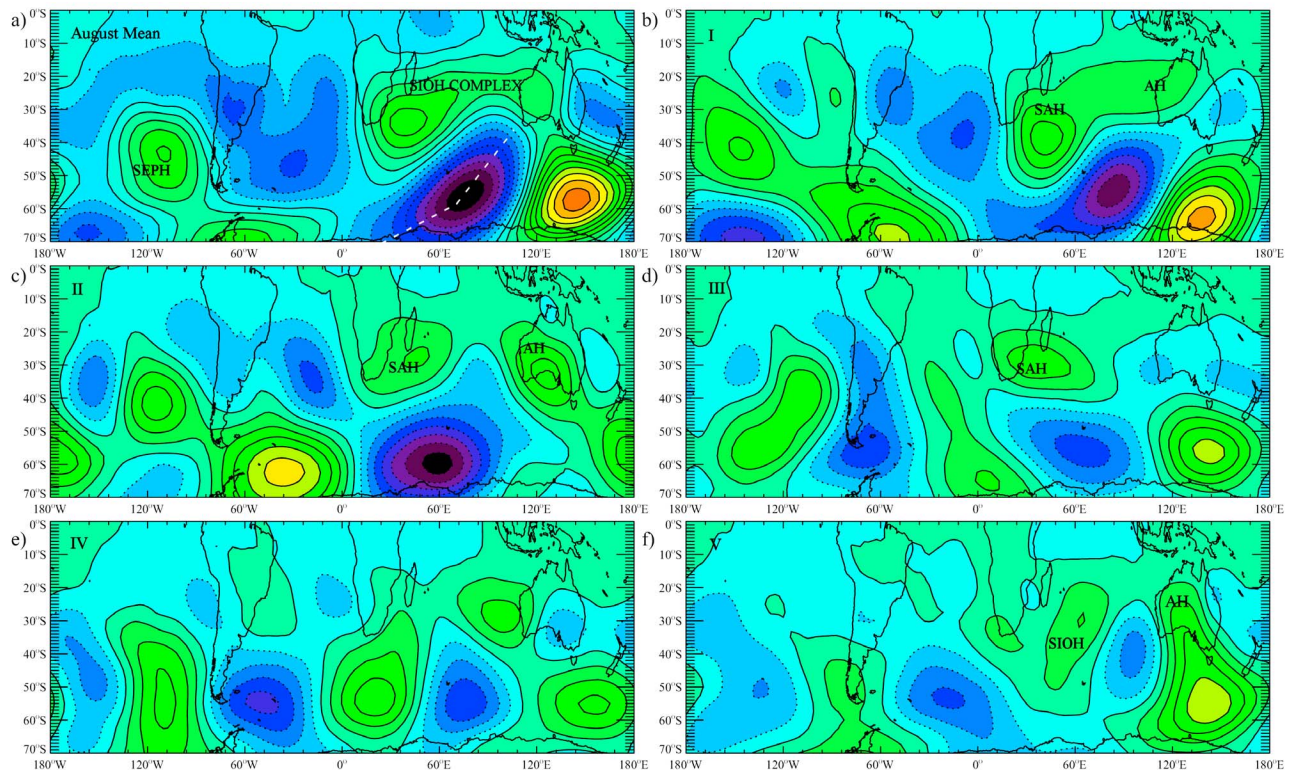


**Figure 6.** Time composite of ECMWF geopotential height anomalies at 150 hPa in the Southern Hemisphere for (a) August 1998 monthly mean, (b) 1–7 August (phase I), (c), 8–11 August (phase II), (d) 12–17 August (phase III), (e) 18–23 August (phase IV), and (f) 24–31 August (phase V). The contour interval is 20m in Figure 6a and 50 m in Figures 6b–6f.

[25] During phase II, 8–11 August, new SAH is visible near 30°E (Figure 5a) and the AH near 110°E is reformed, yielding a two-cell system (Figure 6c). In phase III (12–17 August) these features are no longer present, but the South African High (SAH) is well established in the band 10°W–50°E (Figure 6d). The demise of the SAH at the beginning of phase IV on 18 August (Figure 5a) marks the return of the IOH as the strongest anticyclonic feature at this latitude. Finally, the fifth phase of the month analyzed starts on 24 August with the reestablishment of the AH and a pronounced SIOH as the dominant pair of anticyclones. The categorization of geopotential height and ozone into five distinctive subsets containing similar synoptic situations allows for clearer tracing of the dynamical origins of the positive column ozone anomalies associated with anticyclones in the SH.

[26] At 35°S the flow is predominantly westerly, with cyclones and anticyclones traveling eastward at ~15 m/s (Figure 5b). The eastern Pacific contains more stationary anticyclones, notably near 110°W, the Eastern Pacific High (EPH; see Figure 6a). As the AH migrates westward during the first half of the month at 20°S, stalled amplifying anticyclonic structures are seen near South Africa at 35°S, between 20° and 50°E, peaking on 5 and 13 August (Figure 5b). In general, in the eastern hemisphere there is a moderate correspondence between amplifying anticyclones near 20°S and the stalling and amplification of anticyclones just to the southeast, near 35°S (Figures 5a and 5b). Poleward flow to the west of subtropical anticyclones will advect

tropical PV air into the SH midlatitude westerlies, tending to amplify and stall the eastward progression of traveling anticyclones in the westerlies.

[27] The Hovmöller diagram of geopotential height at 35°S shows importance of the subtropical SAH and AH in coupling of SH tropics with higher-latitude (Figure 5b) wave structure. During 1–15 August, ozone-rich traveling troughs near 50°S (Figure 5c, indicated by dashed line; compare column ozone in Figure 5d) tend to stall and amplify, immediately poleward and downstream of the SAH (Figures 5a and 5b). This leads to a broad quasi-stationary middle- and high-latitude trough located between 0° and 120°E (Figures 6a–6c), which projects strong signal into a monthly mean (Figure 6a). A weaker version of this combination is seen in late August (Figures 6e and 6f). The almost exact collocation of column ozone maxima is visible when comparing the geographical extent of geopotential height anomalies at 50°S (Figure 5c) and their development with time with the life cycle of column ozone at 50°S (Figure 5d). Positions of column ozone maxima accurately match the locations of deep troughs south and southwest of Australia.

[28] When comparing eddy heights (Figure 6a) with TOMS time mean column ozone from August 1998 (Figure 7a), the monthly mean position of the ozone maximum coincides with the trough, and the 300 DU isoline (thicker contour) is roughly collocated with the southern and southeastern boundaries of the positive anomaly. However, using the five phase division described earlier reveals changes in the

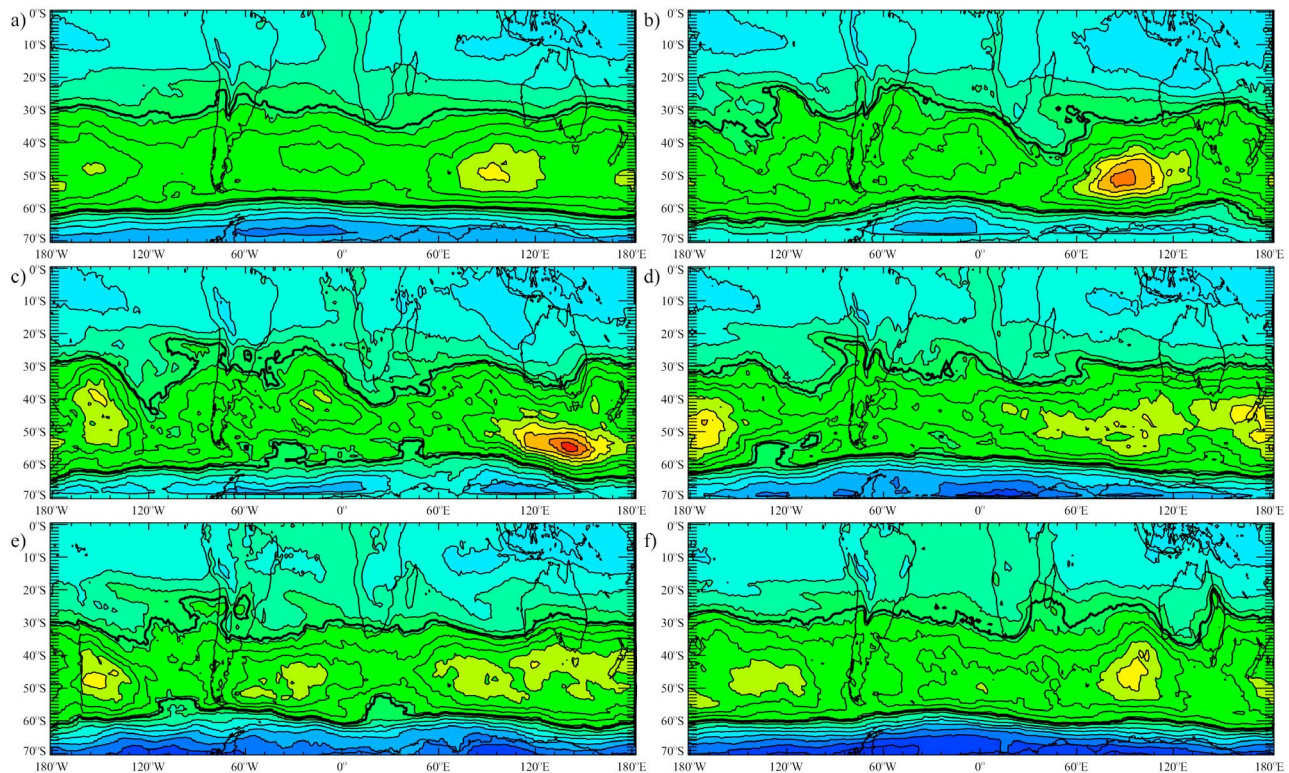


**Figure 7.** Time composite of TOMS column ozone in the Southern Hemisphere for (a) August 1998 monthly mean, (b) 1–7 August (phase I), (c) 8–11 August (phase II), (d) 12–17 August (phase III), (e) 18–23 August (phase IV), and (f) 24–31 August (phase V). The contour interval is 15 DU in Figures 7a–7f.

strength, position and relative importance of both geopotential height disturbances and column ozone extremes.

### 3.1. Phase I

[29] During phase I (Figure 6b) there is an amplified SAH and broad positive anomaly stretching over the Indian Ocean northeastward to the AH. Maxima over the Weddell Sea, Victoria Land, and the Eastern South Pacific High are relatively strong. Column ozone tends to reach its maximum concentration in the center of the trough between the SAH and the anticyclone to the south of Australia (Figure 7b). The 300 DU contour traces the SAH, displaying filament of higher ozone masses wrapped around this time-mean anticyclone, with a signal similar to the PV filaments associated with wave breaking at these latitudes [Hitchman and Huesmann, 2007, 2009]. The 300 DU isoline also surrounds the Eastern Pacific High, with a similar wave-breaking meridional gradient reversal.

[30] To further understanding of the origins of air entering the Australian Subtropical Westerly Jet (ASWJ) just south of the AH we have calculated isentropic trajectories using the LaRC trajectory model described previously. Analysis of isentropic back trajectories identified the latitudinal extent of areas influenced directly by inflow from the TH. Four main sets of parcels were initialized in areas associated with IOH anticyclones at 12°S, 80–87°E (Figure 8a) 22°S, 80–87°E (Figure 8b) and the AH system at 12°S, 107–114°E (Figure 8c) and 22°S, 107–114°E (Figure 8d) on the 360 K isentropic surface. These air parcels were then advected back in time

for 12 days, starting from 5 August 1998, during the first phase of our analysis.

[31] Air parcels that were initialized in an area influenced by the IOH (12°S) originated within NH circulatory systems (Figure 8a), such as those in the TH and highs over the Arabian Peninsula. However, parcels initialized at 22°S had more diverse origins, some making their way to the IOH from the convective zones over Africa and Amazonia, and a few originated over SE Asia (Figure 8b).

[32] Unlike their counterparts, parcels arriving at the western boundary of the AH (Figures 8c and 8d) originated well within the NH TH system's circulation. This supports the idea that the TH-AH coupling plays a major role in the cross-equatorial transport of air. Notable are parcel trajectories (Figures 8a and 8c) collocated with the higher ozone mixing ratio patch crossing the Philippines southwestward across the equator over Sumatra in the 100 hPa Mercator projection of GMAO ozone (Figure 3).

[33] The results of back-trajectory calculations using the isentropic model showed the initial part of the mechanism being studied in this paper; the buildup or magnification of the anticyclonic system over the Australia by infusion of air masses from the TH north of the equator. These air masses themselves are characterized by relatively low-ozone content, but they are instrumental for the setting up of dynamical conditions, namely the magnification of the AH and the trough immediately southeast of it, leading to enhanced transport of air from subtropical regions in the SH stratosphere, which are rich in ozone.

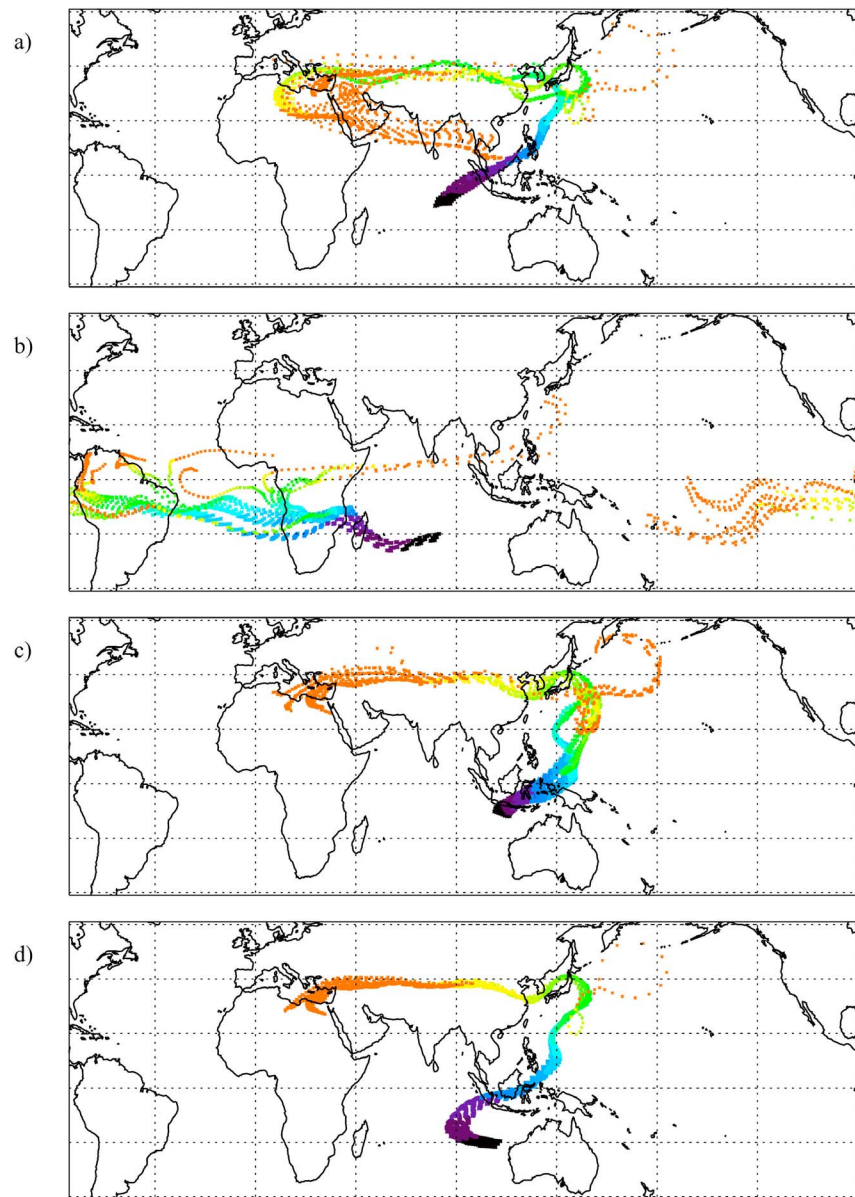


**Figure 8.** Twelve-day back trajectories, at 360 K, for air parcels arriving on 5 August 1998 at (a) 12°S, 80–87°E; (b) 22°S, 80–87°E; (c) 12°S, 107–114°E; and (d) 22°S, 107–114°E. Color-coded ages are as follows: black (1–2 days), purple (3–4 days), blue (5–6 days), green (7–8 days), yellow (9–10 days), and orange (more than 11 days).

### 3.2. Phases II Through V: Readjustment

[34] Phase II was characterized by a westward extension of the SAH toward the Atlantic, a southward migration of the AH, and a general weakening of the connection across the SIO (Figures 5a and 6c). The high centered over Weddell Sea is much stronger, and its diminished downstream counterpart moved from south of Australia to within the vicinity of the dateline. In addition to changes in the synoptic structure, an altered column ozone distribution is also visible (Figure 7c). The 300 DU isoline has moved northward over the Indian Ocean, tracing the edges of the stronger SAH and AH. The eastward displacement of the Eastern Pacific High left lower ozone (<300 DU) air masses

intruding toward 45°S, 90–140°W. The column ozone maximum now resides just south of the strengthened AH at 50°S, 110–170°E, a southeastward displacement when compared with phase I (Figures 6c and 7c). A secondary maximum, resulting from horizontal advection along the eastern edges of the high system displaced from Victoria Land, is located in a trough at 40°S, between 130°W and 160°W (Figures 6c and 7c).

[35] The phase III (Figures 5a and 6d) geopotential height anomaly field shows a lack of definition of the AH, with the Victoria Land High stronger than in the previous phase. The SAH remains distinguishable, and a trough resides over the Weddell Sea, with ridges over the southern Atlantic

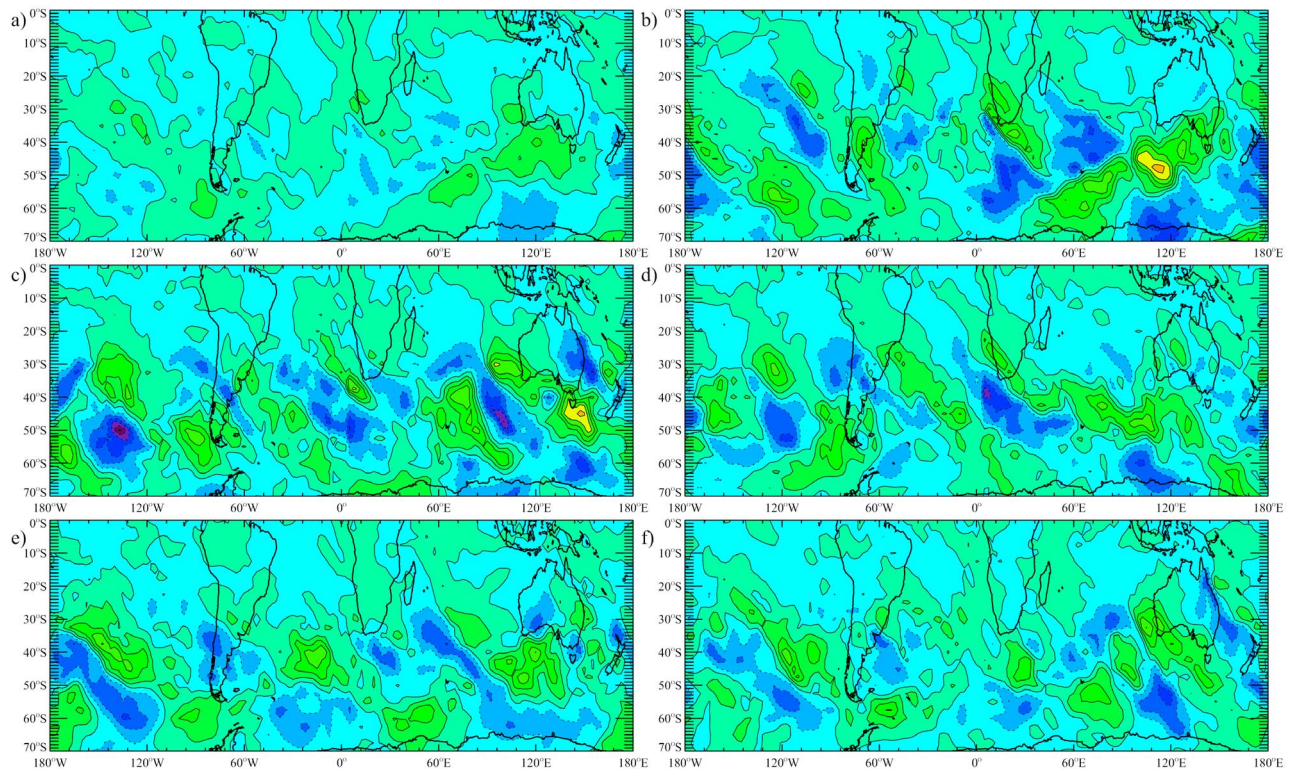


**Figure 9.** Time-composite of 3-D ozone flux convergence at 150 hPa in the Southern Hemisphere for (a) August 1998 monthly mean, (b) 1–7 August (phase I), (c) 8–11 August (phase II), (d) 12–17 August (phase III), (e) 18–23 August (phase IV), and (f) 24–31 August (phase V). The contour interval is 10 ppbv/day in Figures 9a–9f, with positive flux convergence in green and yellow.

and upstream of the Southeastern Pacific High (SEPH). A diminishing ozone maximum is seen to the southeast of the weakening high migrating south of Australia (Figures 6d and 7d). A diffuse ozone maximum is located over the high-latitude SIO in the weakening trough over the coast of Antarctica near 0°E. The 300 DU contour closely traces the longitudinal elongation of the SAH as well as the Southeastern Pacific High.

[36] Panel 6e shows a regenerating AH and a diminished SAH during phase IV (Figure 5a). The anticyclone to the southeast of Australia has weakened and the ozone maximum to its east is becoming more diffuse (Figures 6e and 7e). The eastward traveling baroclinic systems are diffusing ozone eastward, contributing to the monthly mean ozone croissant shape.

[37] In phase V, a weak SIOH has formed, and a focused column ozone maximum is found in the trough immediately to its southeast near 47°S, 80–110°E (Figures 6f and 7f). Again, the 300 DU isoline closely traces the edges of all three anticyclones: the SAH, IOH and AH.

#### 4. Three-Dimensional Large-Scale Ozone Convergence at 150 hPa

[38] Evaluation of the chemical constituent transport equation for the duration of the month of August 1998 allowed us to identify areas of positive flux convergence of ozone associated with combined horizontal and vertical advection. The horizontal ozone convergence into a deep-

ening trough can significantly increase column ozone during a month. Ozone budget computations were designed with the case study as a guide to provide us with first-order approximation of the transport of ozone associated with distinctive synoptic patterns described in the previous chapter. It shows the dependence of ozone concentration on the dynamical transport associated with the life cycle of anticyclones over the Indian Ocean. The vertical component of the left-hand side of the chemical constituent transport equation (equation 1) yielded a magnitude smaller values and less accuracy (small vertical velocities) than horizontal component, underscoring the relative importance of horizontal advection.

[39] The monthly mean ozone flux convergence (Figure 9a) has negative values on the axis drawn between the SAH and the high located around the Weddell Sea (Figure 6a), indicating an area of mean flux divergence (blue). This corresponds to the minimum in TOMS ozone south of Africa, with its axis tilting westward with increasing latitude (Figure 7a). Immediately to the east there is a region of positive flux convergence, indicating a monthly mean influx of ozone which corresponds to creation of the climatological maximum over the Southern Indian Ocean. This feature includes contributions by the mean AH (a positive patch south of Australia), the SAH (on its western time-mean edges), and transport of ozone from the IOH-SAH couplet (60–90°E). Note also the positive flux convergence near the tip of South America, immediately southeast of the Southeast Pacific High.

[40] Since ozone transport depends on synoptic conditions, which differ for the 5 periods identified, analysis of only the monthly mean would be misleading. Phase I (Figure 9b) reveals strong flux convergence associated with enlarged IOH-AH systems, spanning the southern coast of Australia and trending westward with latitude. This pattern contributes strongly to the monthly mean. There is also a strong positive patch at the southwestern edge of the SAH. Flux convergence patterns in the eastern Pacific area are more complicated owing to the combined circulatory effects of the Southern Pacific High, Eastern Pacific High and the anticyclone over the Weddell Sea, all of which produce positive flux convergences on their southwestern edges.

[41] Phase II flux convergence clearly shows a dependence on the distribution of anticyclones (Figure 9c). Strong positive flux convergence west and southeast of Australia results from a well defined AH (Figure 6c) during this time. Strong meridional transport is a dominant feature over the SIO, with positive flux convergences found on the poleward flank of the SAH system. The Eastern Pacific High produces large positive anomalies immediately west of South America and the Weddell Sea High causes advective redistribution of ozone at higher latitudes.

[42] The weakened AH (Figure 6d) diminishes the positive flux convergence south of Australia during 11–17 August (Figure 9d). This leads to a diminished maximum in column ozone, as noted earlier (Figure 7d). The troughs in the southern Pacific and Atlantic, which were displaced eastward during phase III, produce the usual pattern of positive flux convergence associated with their circulation.

[43] During phase IV, the simultaneous resurgence of the AH and demise of the SAH (Figure 6e) immediately changes the distribution of ozone flux convergence in the SH (Figure 9e). The strength of the AH leads to positive patches in the central part of the Indian Ocean and south of Australia. This ozone is then meridionally redistributed by high-latitude systems residing around 55°S (indicated by flux divergence in the Victoria Land High and convergence to the east of this system). By comparing the robust easterly flow in the UTLS region with TOMS ozone data for this time period (Figure 7e), it becomes apparent that meridional advection by high-latitude flow is the main contributor to the elongated maximum observed in the region between Australia and Antarctica.

[44] The return of the SAH and IOH (Figure 6f) is marked by a subsequently stronger positive flux convergence at the Perth-Amery Ice Shelf axis (Figure 9f) along the trough associated with the IOH and a strong influx of ozone south and southwest of Africa (along the southwestern edge of the SAH). The positive flux convergence zones south of the IOH and southwest of the AH are the main contributors to the collocated column ozone maximum (Figure 7f).

[45] The good agreement of flux convergence patterns and column ozone patterns supports the relative importance of dynamical features in producing column ozone distributions on the synoptic scale. Differences arise from the fact that flux convergence is shown near 150 hPa, near the level of maximum ozone convergence, but convergences at other levels contribute to column ozone patterns. The ozone budget study also underscores the importance of horizontal transport into the troughs, with regions located immediately upstream relatively to notable ozone convergence zones

showing areas of strong divergence of similar magnitude. Similarly, the lesser importance of ozone transport by the incoming TH air masses from tropical regions of Maritime Continent (MC) into the area south and southwest of the AH is shown by neutral or only slightly divergent regions over Australia and Indonesia (equatorial and tropical regions of the MC are climatologically marked by column ozone minimum).

## 5. Modeling the TH-AH Coupling With the UWNMS

[46] The temporal and dynamical setup of this mesoscale modeling experiment was designed to explore an idealized situation of increased outflow from the TH into the SH, which in turn modulates the AH extant over the Australian region in the SH. While the outflow itself contributes low-ozone intrusions to the SH UTLS region, our simulation was intended to create a dynamical regime prone to magnifying the AH and increasing transport of ozone rich air masses into the trough south of the perturbed anticyclone.

[47] Climatologically, a zonal wave number 5 pattern emerges as a dominant feature of the extratropical winter UTLS in the band 40°–60°S. The basic state which is being forced is the pressure pattern at 15 km from 4 August 1998 (Figure 10a), which prevails during most of July–October and exhibits a wave 5 aspect. We chose to focus specifically on phase I as an example of forcing the SH flow by outflow from the SIOH system. The cross-equatorial meridional wind component over Singapore indicated a buildup in part of the TH inflow (Figure 2), which we have magnified and used as the forcing in our modeling study. The red shaded area (Figure 10a) shows the extent of the forcing.

[48] During the perturbation spin-up period we observed the formation of poleward flow into the extratropical westerly jet (blue in Figure 10b) and subsequent counterclockwise anticyclonic circulation (solid contours in Figure 10b). This is consistent with quasi-conservation of high potential vorticity from the north. Thus, an anomalous high-pressure system was established to the southwest of Australia (seen here in Figure 10b as a contoured pressure difference between forced and control model runs).

[49] This development was already a robust feature 48 h into the simulation. As with the North Atlantic High studied by *O'Neill and Pope* [1988], the anomalous high became vertically prominent, “growing” into the lower stratosphere. This ridge resulting from the direct outflow from the tropics is collocated with relatively low  $O_3$  mixing ratios. The elongated and deepened trough on the southeast periphery of the anomalous high allowed for more high ozone content air to enter it (Figures 10a and 10b). Figure 11a shows the 0.2 ppmv ozone anomaly isosurface (forced run-control run) colored by pressure, which highlights the vertical extent of the anomaly. The pressure perturbation (the pressure difference between forced and control runs) is shown at 15 km (Figure 11a). The convergence and downward advection of high ozone mixing ratio air into traveling troughs over the higher-latitude SIO leads to increased ozone concentration, and hence, greater column values in the center of the ozone crossant south and southwest of Australia. The vertical extent of intrusions of air masses with a higher ozone mixing ratio is shown in Figure 11b. The positive ozone

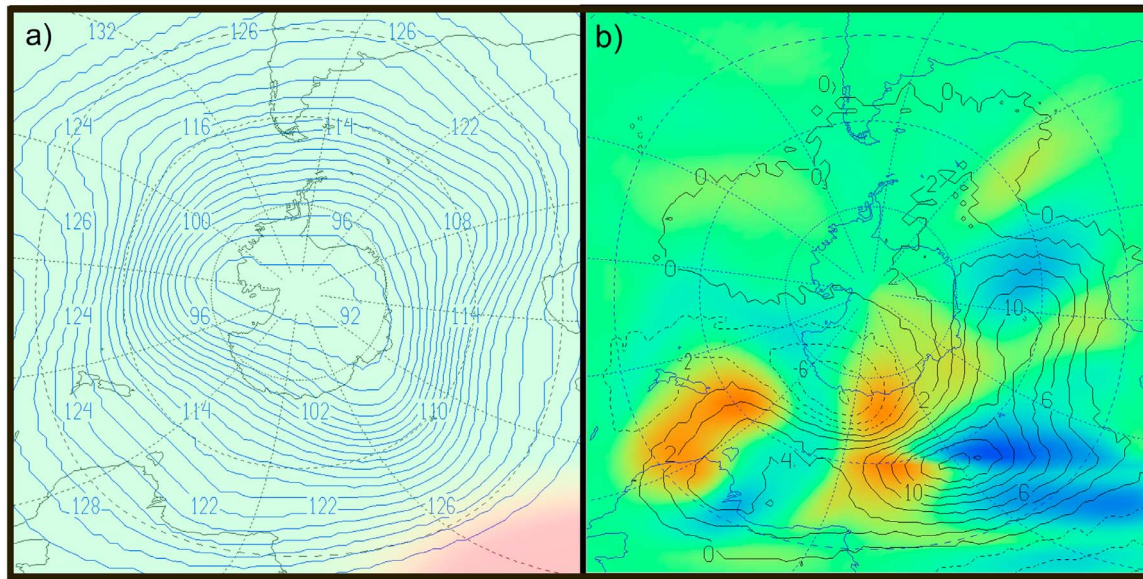


**Figure 10.** Pressure distribution at 15 km (contour interval 2 hPa) in the University of Wisconsin-Madison Nonhydrostatic Modeling System (UWNMS) for (a) the control run at hour 48 of the model run (3 August 1998) and (b) perturbed minus control runs at the same model time after the perturbation achieved its maximum. In Figure 10a the red shading indicates the extent of the wind perturbation. In Figure 10b, dashed lines indicate negative pressure differences, while color indicates meridional velocity difference, with blue (red) indicating more southward (northward) flow in the perturbation. The velocity difference ranges from  $-39$  to  $+36$  m/s.

anomaly located in the trough south of the perturbed anticyclone (marked with a letter A in Figures 11a and 11b) extends well below the 250 hPa level (to 368 hPa), while anomalies denoted as B and C intrude into the 250–150 hPa layer.

[50] After the establishment of the transient anticyclone, the wave train started to travel east and modulated the hemispheric wave pattern, creating a wave number 4 mode. This setup of anticyclonic anomalies projected into wave space as a change from wave number 5 to 4 has been noted in previous observational studies as a recurrent feature of SH dynamics [Wirth, 1991; Trenberth, 1992; Shiotani and Hirota, 1985; Shiotani *et al.*, 1993]. The breadth of the perturbation, being wider than  $L_x = 2\pi \cos 50^\circ \times 6357 \text{ km}/5$  at this latitude, acted to elongate the trough south of Australia. Inspection of the ECMWF data shows that strong inflow events are often precursors to this shift. This situation continued throughout the run. The wave pattern appears to be smoothed by the elongation of the trough (Figures 10b and 11a), with stronger height gradients indicating a more intense westerly jet to the south of the anticyclone. This is consistent with understanding of the secondary circulation around jets, which is poleward and downward into the trough in the UTLS [e.g., Shapiro, 1980]. This is further consistent with the Stokes drift for Rossby waves [Wallace, 1978] and the downward control principle for synoptic waves absorbed in the lower stratosphere [Haynes *et al.*, 1991].

[51] By 72 h there is downstream development of alternating high- and low-pressure perturbations around Antarctica. The zonal phase speed of the resulting wave was close to 30 m/s, which is consistent with the Rossby wave dispersion relation. Consequently, we observed higher

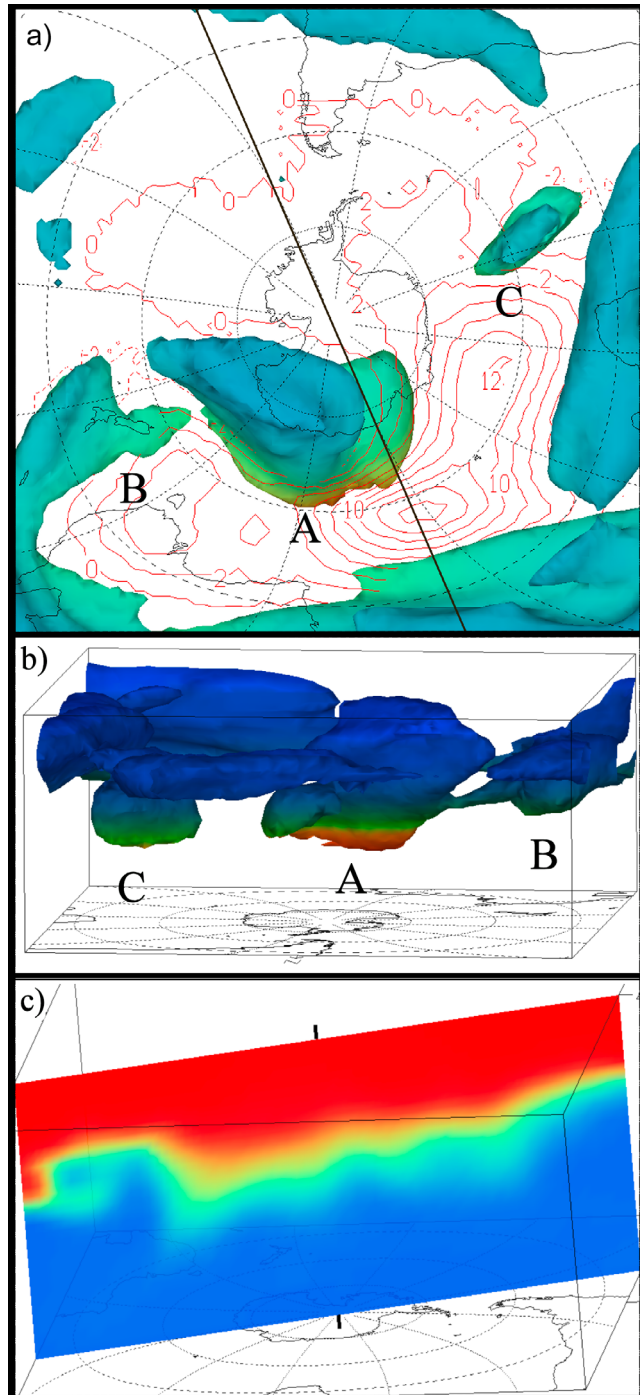
ozone concentrations anchored around these perturbations (Figure 6a), especially at their southeastern edges. A vertical section through the center of anticyclonic perturbation shows an elevated troposphere surrounded by a pattern of ozone-rich air masses around the edges of modeled anticyclone (Figure 11c). The 1.5 ppmv  $\text{O}_3$  contour (light blue to green) extends deep into the troposphere on the southern side of the anomalous anticyclone, while the northern edge is more vertically localized.

[52] Such deep incursions occur many times during one June–November season in the South Indian Ocean/Australian sector. Some of the high ozone content masses are advected eastward, contributing to the elongation of the OM. Monthly means of synoptic snapshots yield the croissant-shaped maximum in column ozone, owing to stratospheric intrusions being more common upstream of and in the maximum.

[53] This general dynamical situation is maintained until inflow from the NH ceases, then the whole downstream wave train slowly decays and wave number 5 is reestablished as the dominant pattern in the SH. In the absence of broad forcing introduced earlier in the run, the circulation adjusts back to the initial wave-five pattern.

[54] To accentuate the pathways associated with the transport of the ozone-rich air parcels we have performed back-trajectory computations using model data. The back trajectories were initialized inside the anomalous ozone maximum in the trough south of the AH on 4 August at the altitude of 15 and 20 km. The air parcels were then advected back in model time to the initialization time. Large portion of parcels initialized at 15 km could be traced back to regions of the subtropical stratosphere over the Indian Ocean, South Africa and east coast of South America in this case study (Figure 12a). Parcels advected from these regions

gradually descend, originating at the heights between 16 and 17 km. Parcels descended  $\sim 1\text{--}2$  km in one week, implying a 1 K/day cooling rate. The back trajectories computed using parcels initialized at the 20 km level (Figure 12b) led to eastern Pacific and South American regions. These results show the sources of transported ozone and other chemical constituents to be far upstream from their final destinations. Much of the ozone climatologically residing in the positive region of the “ozone croissant” is seen to originate over the subtropical Atlantic and Pacific.



[55] The end of the simulation coincides in time with late phase I and the transition from the phase I to II in our synoptic case study (section 3). The observed southward outflow from the TH (Figure 2) increases at the final part of the simulation (5 August and thereafter) providing an anomalous anticyclonic air mass to magnify the AH and increase transport of ozone into the trough southwest of it (Figures 6c and 7c).

## 6. Conclusions

[56] The presented study aimed at an explanation of the dynamical mechanism producing the observed zonally asymmetric distribution of column ozone in the SH during late winter and spring. This multistage dynamical connection between the NH as SH may be summarized as follows:

[57] 1. Outflow from the TH system creates a streamer into the SH, around the AH system.

[58] 2. Southward flow effectively gives in to the effects of rotation and anomalous momentum transported from the NH establishes the ASWJ core [Hitchman and Rogal, 2010a] while amplifying the AH system.

[59] 3. Air masses which are relatively rich in ozone and originating far upstream in the tropical and subtropical SH lower stratosphere descend into the amplified troughs, with the resulting ozone concentration providing for the peculiar asymmetry in column ozone.

[60] A blend of analysis of ECMWF data and modeling assembled together as a case study was presented in order to establish a sufficiently persuasive link between the TH, AH and the OM.

[61] The observational part of the study, which consisted of composite analysis of five periods in August, led to the marking of distinctive modes in the life cycle of SH anticyclones. Via analysis of geopotential height anomalies and ozone flux convergence associated with phases 1–5, we showed the relative importance of the SAH, IOH and AH in the cumulative transport of ozone in the Indian Ocean region, leading to the zonal asymmetry in column ozone distribution. Analysis revealed that the ozone maximum tends to be zonally elongated in the presence of the IOH and SAH systems. In contrast, the presence of a relatively

**Figure 11.** (a) UWNMS perturbation pressure at 15 km (contour interval 2.0 hPa) and +0.2 ppmv ozone anomaly isosurface, colored by pressure, at 1200 UT on 4 August 1998 in the perturbed run. Pressure levels of anomaly isosurfaces range from 448 hPa at 5.8 km (red) to 12.3 hPa at 25.5 km (blue). The black line shows the position of the vertical section shown in Figure 11c, with the South Indian Ocean at left. Letters A, B, and C mark major stratospheric ozone mixing ratio intrusions. (b) Perspective view of +0.2 ppmv ozone anomaly isosurface (same as Figure 11a) showing the vertical extent of ozone intrusions. Blue denotes levels higher than 150 hPa, black 250–150 hPa, and orange levels lower than 250 hPa. (c) Latitude-height section of UWNMS ozone volume mixing ratio and 15 km pressure (contour interval 2 hPa) at 1200 UT on 4 August. The transition zone between blue and red colors denotes values close to 1.5 ppmv. Note the elevated tropopause over the forced anticyclone and ozone streamer into the troposphere on its poleward periphery.

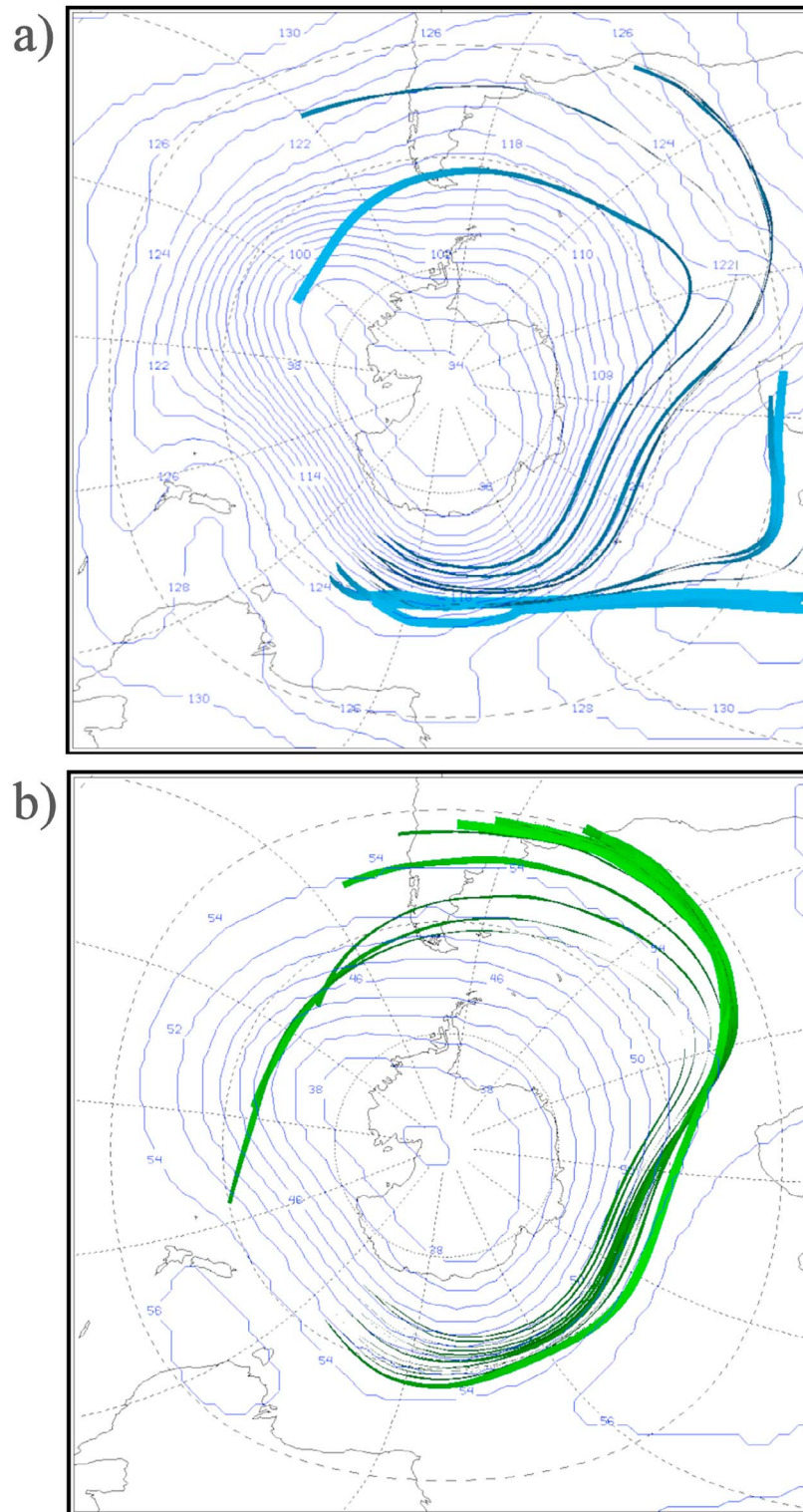


**Figure 12.** UWNMS back trajectories initialized at 1200 UT on 4 August 1998 at (a) 15 km and (b) 20 km.

stronger AH introduces a more zonally limited column ozone maximum (Figures 6d and 7d versus Figures 6f and 7f). We also noted that anticyclones located in the surf zone tend to induce meridional transport of ozone,

while their high-latitude counterparts tend to cause a more zonal redistribution through horizontal advection. Many amplifications of the AH may be further linked to the activity of TH.

[62] The importance of the northern Gill [1980] solution to off-equatorial transient heating owing to convection (namely the Tibetan High) was highlighted through use of trajectory analysis. This part of the study showed that a significant amount of air reaching the SH subtropical westerlies over the SIO originated well within the NH, sometimes inside the TH circulation zone. The meridional transport of air masses, linked in this study with the outflow from the TH, is well known from the classic concept of monsoonal circulations [Shaw, 1930], where mass circulation occurs by upward vertical mass transport in the region of net heating and downward mass transport in the cooling regions. Mass continuity requires a quasi-horizontal mass transport from the heat source to heat sink in the upper branches with corresponding reversed transport below. Net horizontal transports of momentum, entropy and energy are necessary for the equilibration of the atmospheric time-averaged thermal structure in relation to the observed heat sources and sinks [Townsend and Johnson, 1981; Johnson, 1980, 1989] and result in the development of isentropic mass circulations [Johnson et al., 1982; Schaack, 1982; Hoerling and Johnson, 1986].

[63] The second part of this study focused on modeling the southern part of the major cross-equatorial dynamical connection between two of the most prominent quasi-stationary anticyclones in the Indian Ocean region: the Tibetan High and Australian High. We have tested the model's response to lateral inflow in the UTLS, the mechanism hypothesized to be responsible for the dynamical redistribution of ozone in the SH. The direct wind forcing used in these simulations provided a novel and robust way to model the impact of the boreal summer monsoon outflow on the SH. It is the instigating mechanism for the modulation of the SH wave train.

[64] Climatologically, in the southern subtropics ( $\sim 13^{\circ}\text{S}$ ; see Figure 4a), quasistationary anticyclones occur near Africa ( $20^{\circ}\text{E}$ ) and South America ( $50^{\circ}\text{W}$ ), and especially near Australia ( $110^{\circ}\text{E}$ ). In the NH, differences in the continentality alter the distribution of quasi-stationary anticyclones somewhat. During late summer and fall the TH is the most prominent anticyclonic feature in our atmosphere (Figure 4b, around  $40\text{--}120^{\circ}\text{E}$ ). The climatological existence of the AH near  $110^{\circ}\text{E}$  in the SH and the TH over the Tibetan Plateau was partially explained by Gill [1980]. Established as a direct outcome of convective forcing, the AH is heavily modulated by direct connection with its stationary counterpart in the NH, the Tibetan High.

[65] The geographical location of these mutually connected anticyclones, and their prevalent dynamical coupling, introduces a peculiar shape in the total ozone distribution climatology (as seen from analysis and through the modeling study), since downward transport of high ozone content air is especially strong in the deep troughs on the periphery of these growing Indian Ocean anticyclones. This two-step study provides insight into the mechanisms governing synoptic ozone distributions in the SH. It may supplement the abundance of documented, well established teleconnection patterns [e.g., Wallace and Gutzler, 1981; Hines and Bromwich, 2002] in an effort to explain some of our planet's dynamic variability and distribution of constituents.

[66] **Acknowledgments.** This work was supported by NSF grant ATM-0822858 and NASA grant NNX08AW52G. We thank Elizabeth Klusinske for help in preparing the manuscript.

## References

- Andrews, D. G., J. R. Holton, and C. B. Leovy (1987), *Middle Atmosphere Dynamics*, Academic, New York.
- Brasseur, G. P., and S. Solomon (1986), *Aeronomy of the Middle Atmosphere*, 2nd ed., D. Reidel Publ., Dordrecht.
- Butcher, J. C. (1987), *The Numerical Analysis of Ordinary Differential Equations: Runge-Kutta and General Linear Methods*, John Wiley, New York.
- Gill, A. E. (1980), Some simple solutions for heat-induced tropical circulation, *Q. J. R. Meteorol. Soc.*, *106*, 447–462, doi:10.1002/qj.49710644905.
- Harvey, V. L., R. B. Pierce, M. H. Hitchman, C. E. Randall, and T. D. Fairlie (2004), On the distribution of ozone in stratospheric anticyclones, *J. Geophys. Res.*, *109*, D24308, doi:10.1029/2004JD004992.
- Haynes, P. H., C. J. Marks, M. E. McIntyre, T. G. Shepherd, and K. P. Shine (1991), On the “downward control” of extratropical diabatic circulations by eddy-induced mean zonal forces, *J. Atmos. Sci.*, *48*, 651–678, doi:10.1175/1520-0469(1991)048<0651:OTCOED>2.0.CO;2.
- Hines, K. M., and D. H. Bromwich (2002), A pole to pole to pole west Pacific atmospheric teleconnection during August, *J. Geophys. Res.*, *107*(D18), 4359, doi:10.1029/2001JD001335.
- Hitchman, M. H., and A. S. Huesmann (2007), A seasonal climatology of Rossby wave breaking in the layer 330–2000 K, *J. Atmos. Sci.*, *64*, 1922–1940, doi:10.1175/JAS3927.1.
- Hitchman, M. H., and A. S. Huesmann (2009), Effect of the quasi-biennial oscillation on Rossby wave breaking in the stratosphere and tropopause layer, *J. Atmos. Sci.*, *66*, 935–946.
- Hitchman, M. H., and M. J. Rogal (2010a), Influence of tropical convection on the Southern Hemisphere ozone maximum during the winter to spring transition, *J. Geophys. Res.*, *115*, D14118, doi:10.1029/2009JD012833.
- Hitchman, M. H., and M. J. Rogal (2010b), ENSO influences on monthly mean column ozone and stratospheric geopotential height and temperature anomalies during the Southern Hemisphere winter to spring transition, *J. Geophys. Res.*, doi:10.1029/2009JD012844, in press.
- Hoerling, M. P., and D. R. Johnson (1986), On the maintenance of the semi-permanent centers of action during January 1979, *National Conference — Scientific Results of the First GARP Global Experiment, Miami, Fla., 1986*, pp. 91–94, Am. Meteorol. Soc., Boston, Mass.
- Hollingsworth, A., D. B. Shaw, P. Lönnberg, L. Illari, K. Arpe, and A. J. Simmons (1986), Monitoring of observation and analysis quality by a data assimilation system, *Mon. Weather Rev.*, *114*, 861–879, doi:10.1175/1520-0493(1986)114<0861:MOOAAQ>2.0.CO;2.
- Hudson, R. D., A. D. Frolov, M. F. Andrade, and M. B. Follette (2003), The total ozone field separated into meteorological regimes, part 1: Defining the regimes, *J. Atmos. Sci.*, *60*, 1669–1677, doi:10.1175/1520-0469(2003)060<1669:TTOFSI>2.0.CO;2.
- Huesmann, A., and M. H. Hitchman (2001), The stratospheric quasi-biennial oscillation in the NCEP reanalyses: Climatological structures, *J. Geophys. Res.*, *106*, 11,859–11,870.
- Johnson, D. R. (1980), A generalized transport equation for use with meteorological coordinate systems, *Mon. Weather Rev.*, *108*, 733–745, doi:10.1175/1520-0493(1980)108<0733:AGTEFU>2.0.CO;2.
- Johnson, D. R. (1989), The forcing and maintenance of global monsoonal circulations: An isentropic analysis, *Adv. Geophys.*, *31*, 43–316.
- Johnson, D. R., M. Y. Wei, and T. Schaack (1982), Planetary-scale mass, momentum and energy exchange, paper presented at Int. Conf. on the Sci. Results of the Monsoon Exp., Denpasar, Bali, 26–30 October, pp. 240–243, World Meteorol. Org., Geneva, Switzerland.
- Newman, P. A., and W. J. Randel (1988), Coherent ozone-dynamical changes during the Southern Hemisphere spring, 1979–1986, *J. Geophys. Res.*, *93*, 12,585–12,606, doi:10.1029/JD093iD10p12585.
- O'Neill, A., and V. D. Pope (1988), Simulations of linear and nonlinear disturbances in the stratosphere, *Q. J. R. Meteorol. Soc.*, *114*, 1063–1110, doi:10.1002/qj.49711448210.
- Orsolini, Y., D. Cariolle, and M. Deque (1995), Ridge formation in the lower stratosphere and its influence on ozone transport: A general circulation model study during late January 1992, *J. Geophys. Res.*, *100*, 11,113–11,135, doi:10.1029/94JD01930.
- Orsolini, Y. J., D. B. Stephenson, and F. J. Doblas-Reyes (1998), Storm track signature in the total ozone during Northern Hemisphere winter, *Geophys. Res. Lett.*, *25*, 2413–2416, doi:10.1029/98GL01852.
- Pierce, R. B., and T. D. Fairlie (1993), Chaotic advection in the stratosphere: Implications for the dispersal of chemically perturbed air from

- the polar vortex, *J. Geophys. Res.*, *98*, 18,589–18,595, doi:10.1029/93JD01619.
- Pokrandt, P. J., G. J. Tripoli, and D. D. Houghton (1996), Processes leading to the formation of mesoscale waves in the midwest cyclone of 15 December 1987, *Mon. Weather Rev.*, *124*, 2726–2752, doi:10.1175/1520-0493(1996)124<2726:PLTTFO>2.0.CO;2.
- Postel, G. A., and M. H. Hitchman (2001), Observational diagnosis of a Rossby wave breaking event along the subtropical tropopause, *Mon. Weather Rev.*, *129*, 2555–2569.
- Randel, W. J., and J. B. Cobb (1994), Coherent variations of monthly mean total ozone and lower stratospheric temperature, *J. Geophys. Res.*, *99*, 5433–5447, doi:10.1029/93JD03454.
- Randel, W. J., and M. Park (2006), Deep convective influence on the Asian summer monsoon anticyclone and associated tracer variability observed with Atmospheric Infrared Sounder (AIRS), *J. Geophys. Res.*, *111*, D12314, doi:10.1029/2005JD006490.
- Randel, W. J., F. Wu, and R. Stolarski (2002), Changes in column ozone correlated with the stratospheric EP flux, *J. Meteorol. Soc. Jpn.*, *80*, 849–862.
- Sardeshmukh, P. D., and B. J. Hoskins (1988), The generation of global rotational flow by steady idealized tropical divergence, *J. Atmos. Sci.*, *45*, 1228–1251, doi:10.1175/1520-0469(1988)045<1228:TGOGRF>2.0.CO;2.
- Schaack, T. K. (1982), The global angular momentum balance for January 1979, *Publ. 09(82), SI*, Dept. of Meteorol., Univ. of Wisc., Madison.
- Schubert, S. D., and M. J. Munteanu (1988), An analysis of tropopause pressure and total ozone correlations, *Mon. Weather Rev.*, *116*, 569–582, doi:10.1175/1520-0493(1988)116<0569:AAOTPA>2.0.CO;2.
- Shapiro, M. A. (1978), Further evidence of mesoscale and turbulent structure of upper jet stream-frontal zone systems, *Mon. Weather Rev.*, *106*, 1101–1111.
- Shapiro, M. A. (1980), Turbulent mixing within tropopause folds as a mechanism for the exchange of chemical constituents between the stratosphere and troposphere, *J. Atmos. Sci.*, *37*, 994–1004, doi:10.1175/1520-0469(1980)037<0994:TMWTFA>2.0.CO;2.
- Shaw, N. (1930), *Manual of Meteorology*, vol. III, *The Physical Processes of Weather*, Cambridge Univ. Press, New York.
- Shiotani, M., and I. Hirota (1985), Planetary wave-mean flow interaction in the stratosphere: A comparison between Northern and Southern Hemisphere, *Q. J. R. Meteorol. Soc.*, *111*, 309–334, doi:10.1256/smsqj.46803.
- Shiotani, M., N. Shimoda, and I. Hirota (1993), Inter-annual variability of the stratospheric circulation in the Southern Hemisphere, *Q. J. R. Meteorol. Soc.*, *119*, 531–546, doi:10.1002/qj.49711951110.
- Solomon, S., R. R. Garcia, F. S. Rowland, and D. J. Wuebbles (1986), On the depletion of Antarctic ozone, *Nature*, *321*, 755–758.
- Stajner, I., and K. Wargan (2004), Antarctic stratospheric ozone from the assimilation of occultation data, *Geophys. Res. Lett.*, *31*, L18108, doi:10.1029/2004GL020846.
- Stajner, I., L. P. Riishojgaard, and R. B. Rood (2001), The GEOS ozone data assimilation system: Specification of error statistics, *Q. J. R. Meteorol. Soc.*, *127*, 1069–1094.
- Stajner, I., K. Wargan, L.-P. Chang, H. Hayashi, S. Pawson, and H. Nakajima (2006), Assimilation of ozone profiles from the Improved Limb Atmospheric Spectrometer-II: Study of Antarctic ozone, *J. Geophys. Res.*, *111*, D11S14, doi:10.1029/2005JD006448.
- Townsend, R. D., and D. R. Johnson (1981), The mass and angular momentum balance of the zonally averaged global circulation, paper presented at *ICSU/WMO GARP Conf. Proc. Int. Conf. Prelim. FGGE Data Anal. Results, Bergen, Norway, World Meteorol. Organ.*, Geneva.
- Trenberth, K. (1992), Global analyses from ECMWF and atlas of 1000 to 10 mb circulation statistics, *NCAR Tech. Note-373+STR*, 205 pp., Natl. Cent. for Atmos. Res., Boulder, Colo.
- Tripoli, G. J. (1992), A nonhydrostatic mesoscale model designed to simulate scale interaction, *Mon. Weather Rev.*, *120*, 1342–1359, doi:10.1175/1520-0493(1992)120<1342:ANMMDT>2.0.CO;2.
- Wallace, J. M. (1978), Trajectory slopes, countergradient heat fluxes and mixing by lower stratospheric waves, *J. Atmos. Sci.*, *35*, 554–558, doi:10.1175/1520-0469(1978)035<0554:TSCHFA>2.0.CO;2.
- Wallace, J. M., and D. S. Gutzler (1981), Teleconnections in the geopotential height field during the Northern Hemisphere winter, *Mon. Weather Rev.*, *109*, 784–812, doi:10.1175/1520-0493(1981)109<0784:TITGHF>2.0.CO;2.
- Webster, P. J. (1972), Response of the tropical atmosphere to local, steady forcing, *Mon. Weather Rev.*, *100*, 518–541, doi:10.1175/1520-0493(1972)100<0518:ROTTAT>2.3.CO;2.
- Wirth, V. (1991), What causes the seasonal cycle of stationary planetary waves in the southern stratosphere?, *J. Atmos. Sci.*, *48*, 1194–1200, doi:10.1175/1520-0469(1991)048<1194:WCTSCO>2.0.CO;2.
- Wirth, V. (1993), Quasi-stationary planetary waves in total ozone and their correlation with lower stratospheric temperature, *J. Geophys. Res.*, *98*, 8873–8882, doi:10.1029/92JD02820.

M. L. Buker, Department of Geography, Western Illinois University, Macomb, IL 61455, USA.

H. Hayashi, Research Institute for Sustainable Humanosphere, Kyoto University, Gokasho, Uji, Kyoto 611-0011, Japan.

M. H. Hitchman, M. Rogal, and G. J. Tripoli, Atmospheric and Oceanic Sciences Department, University of Wisconsin-Madison, 1225 West Dayton St., Madison, WI 53706, USA. (mjrogal@wisc.edu)

I. Stajner, Noblis, Falls Church, VA 22042, USA.